Large Eddy Simulations of turbulent particle-laden channel flow

CrossMark

George Mallouppas, Berend van Wachem *

Division of Thermofluids, Department of Mechanical Engineering, Imperial College London, Exhibition Road, London SW7 2AZ, United Kingdom

A B S T R A C T

This paper scrutinises the Large Eddy Simulation (LES) approach to simulate the behaviour of inter-acting particles in a turbulent channel flow. A series of simulations that are fully (four-way), two-way and one-way coupled are performed in order to investigate the importance of the individual physical phenomena occurring in particle-laden flows. Moreover, the soft sphere and hard sphere models, which describe the interaction between colliding particles, are compared with each other and the drawbacks and advantages of each algorithm are discussed. Different models to describe the sub-grid scale stresses with LES are compared. Finally, simulations accounting for the rough walls of the channel are compared to simulations with smooth walls. The results of the simulations are discussed with the aid of the experimental data of Kussin J. and Sommerfeld M., 2002, *Experimental studies on particle behaviour and turbulence modification in horizontal channel flow with different wall roughness, Exp. in Fluids, 33, pp. 143–159* of Reynolds number 42,000 based on the full channel height. The simulations are carried out in a three-dimensional domain of 0.175 m × 0.035 m × 0.035 m where the direction of gravity is perpendicular to the flow. The simulation results demonstrate that rough walls and inter-particle collisions have an important effect in redistributing the particles across the channel, even for very dilute flows. A new roughness model is proposed which takes into account the fact that a collision in the soft sphere model is fully resolved and it is shown that the new model is in very good agreement with the available experimental data.

© 2013 Elsevier Ltd. All rights reserved.

1. Introduction

Particle-laden turbulent flows can be found in various industrial and environmental processes. Examples of such processes are pneumatic transport of particles; energy conversion of fossil fuels; movement of soot particles in the atmosphere; the flow of particles in cyclones and many more. Understanding the effects of particle–fluid interactions is of utmost importance because this will result in a more accurate implementation of these processes. Additionally, applications such as sediment transport, where the direction of gravity is perpendicular to the flow, particle–particle and particle–wall collisions become very important. Therefore, the need to understand the effects of these additional physical phenomena is of fundamental importance. Thus robust numerical simulations will therefore help the optimisation and better design of industrial processes and provide a more reliable prediction of environmental processes involving particles.

There are various frameworks in which the continuous phase for gas–solid flows can be predicted, i.e. Direct Numerical Simulation (DNS), Large Eddy Simulation (LES) and the Reynolds Averaged Navier–Stokes (RANS) method. DNS methods offer high accuracy in resolving all scales without ad hoc modelling at the expense of

huge computational time. Currently, DNS can only solve flows of relatively low Reynolds (*Re*) numbers, which are outside of most engineering and industrial interests. Although the computational effort for LES is still very high, it is considerably lower than for DNS and it has therefore become very fashionable for analysing flows in academia and it is also an emerging tool in industry.

LES solves the Navier–Stokes equations up to a particular length-scale due to the application of a filter. Length-scales smaller than the cut-off filter width (Δ) are modelled with a so-called sub-grid scale (SGS) model. The cut-off width is an indication of the smallest size eddies that are retained in the computations and eddies smaller than Δ, are filtered out. Due to the filtering of the Navier–Stokes equations, models are required to provide closure for the SGS stresses, which account for the effect of the unresolved scales on the convective momentum transport. In this paper, the well known model proposed by Smagorinsky (1963) with van Driest damping near the wall is used to model the SGS stresses. Moreover, the model proposed by Germano et al. (1991) and Lilly (1992) is also adopted. The results of the two LES models are compared with each other in order to verify that the solutions are independent from the SGS models.

There are various frameworks to model the collisions between particles; via stochastic or deterministic methods. Stochastic methods, such as the one proposed by Sommerfeld (2001), generate fictitious collision partners with a given size and velocity and as

* Corresponding author. Tel.: +44 20 7594 7030; fax: +44 20 7581 5495.
  E-mail address: Berend.van.Wachem@gmail.com (B. van Wachem).

a result no information regarding the real position and velocity of the particles and the corresponding fluid environment is required. Stochastic collisions are therefore performed via the use of a probability density function which is based on kinetic theory. The benefit of this method is the speed of computation of the collisions because no collision pairs are searched within the domain. However, the downside of these methods is that the particle and fluid velocity fluctuations need to be assumed (e.g. Gaussian) and this may prevent the prediction of clustering. Deterministic methods on the other hand, determine collision pairs by using the particles actual position and velocity. The actual collisions can be performed either by the soft sphere or hard sphere model. In this work the particle interactions are modelled according to the soft sphere and the hard sphere models, which are both deterministic methods, in order to investigate their main differences.

In the soft sphere model, first applied by Cundall and Strack (1979), the collisions are approximated by the elastic and plastic deformation on the particle–particle contact area occurring during a collision. Such a deformation can be mathematically described by a spring-dashpot-slider model (Tsuji et al., 1992). On the other hand, the hard sphere model, which was first proposed by Maw et al. (1976) and further developed by Louge (1994), uses the conservation of momentum of the particles and approximates the collisions as instantaneous and binary. In other words, the hard sphere collisions are event-driven, as opposed to the soft sphere model which uses a fixed time-step, and hence this makes the large scale simulations potentially faster. Note, however, this is only valid for fast flowing dilute flows where the errors of the hard sphere model approximations are negligible. In addition, in these type of simulations, a large number of particles are required. The soft sphere approach is computationally more intensive compared to the hard sphere model because the collision of each particle is fully resolved. On the other hand, the soft sphere model potentially has a higher accuracy as no empirical data, besides the material properties, are required to compute the collisions.

In this work, the point-particle or point-mass approach is used to approximate the presence of particles as seen by the fluid. The effect of the particles on the fluid phase is modelled as an inter-phase momentum exchange source term. Elghobashi and Truesdell (1992) mention that the point-particle approach is valid if the particle diameter (d_p) is smaller than the Kolmogorov scale (η_κ). This implies that d_p must be smaller than the grid size (Δx). Although accounting for the volume fraction effects on the drag force is probably not of large importance in the test-cases simulated in the current research work, it might have an effect on the particle-clustering. Individual particles are tracked by solving Newton's second law. Moreover, the drag force of the fluid acting on the particles is added via the correlation proposed by Wen and Yu (1966). Therefore the simulations performed in this work are fully coupled, or four-way coupled.

The purpose of this paper is to examine the particle behaviour in a horizontal channel flow with the gravity acting perpendicular to the main flow direction. This paper first compares the hard sphere and soft sphere methodologies and evaluates their differences as opposed to other studies that primarily use the hard sphere methodology, such as Sommerfeld (2003). The results of the two models are compared to the experiment of Kussin and Sommerfeld (2002), who investigate the particle behaviour and turbulence modification of a horizontal channel flow. Finally, this article investigates the differences and effects of simulations that are one-way coupled, two-way coupled and four-way coupled on the particle statistics. Moreover, the effect of the wall roughness on the particle statistics is investigated and compared to the available experimental data and a novel wall roughness model that is used in conjunction with the soft sphere methodology is proposed.

This paper is organised in six sections. Section 2 describes how the fluid-phase is solved and how the fluid sub-grid scales are modelled. Section 3 describes how the equation of motion for each particle is solved, the method used for particle tracking and the models used for the wall roughness for both the soft sphere and hard sphere models are discussed. Section 4 describes the simulation set-up and Section 5 compares and discusses the numerical results with the available experimental data and various set-up conditions. Section 6 summarises the main conclusions of this work.

2. Fluid-phase modelling

2.1. Large Eddy Simulation

The filtered momentum equation for the fluid phase is

$$\frac{\partial(\alpha_f \rho_f \tilde{v}_{f,j})}{\partial t} + \frac{\partial(\alpha_f \rho_f \tilde{v}_{f,j} \tilde{v}_{f,i})}{\partial x_i} = -\alpha_f \frac{\partial \tilde{p}}{\partial x_j} + \frac{\partial(\alpha_f \tilde{\tau}_{ij})}{\partial x_i} - \frac{\partial\left(\alpha_f \tau_{ij}^a\right)}{\partial x_i} \\ + S_{f,j} + \sum_{p=1}^{phases \neq f} \beta_{(f,p)}[\tilde{v}_{f@p,j} - v_{p,j}] \qquad (1)$$

where α_f is the fluid volume fraction, ρ_f is the fluid density and $\tilde{v}_{f,i}$ is the filtered fluid velocity. The last two terms on the right hand side of Eq. (1) are source terms; $S_{f,j}$ is an additional source term; and $\sum_{p=1}^{phases \neq f} \beta_{(f,p)}[\tilde{v}_{f@p,j} - v_{p,j}]$ is the inter-phase momentum exchange between the two phases respectively; the subscript $f@p$ indicates the undisturbed fluid at the location of the particle. For more details and validation see Electronic Annex A in the online version of this article.

2.1.1. Periodic conditions and driving pressure drop

As the domain is periodic in the direction of the flow an additional source term is required to drive it. This source term is equal to the integrated wall shear stress. This additional source term is added in the filtered momentum equation, analogously to the pressure drop. Furthermore, there are two ways to implement this: (a) by fixing the mass flow rate $\dot{m}$, which will be corrected by adjusting the forcing term in the momentum equation at every time-step; and (b) by specifying a constant pressure gradient (dp/dx), which can be applied when the required wall shear stress is known.

The former has been used in the current simulation which results in

$$S_{f,1} = \frac{\dot{m}_o - \dot{m}_n}{A_{cross} \Delta t_n} \qquad (2)$$

where $\dot{m}_o$ is the specified mass flow rate at a given cross-section; $\dot{m}_n$ is the computed mass flow rate at current time step; A_{cross} is the cross-sectional area; and Δt_n is the current time-step. $S_{f,1}$ has the units of pressure gradient; i.e. $\frac{kg}{m^2 s^2}$. Note that this is only implemented in the x-direction, $S_{f,2}$ and $S_{f,3}$ are zero, as there is no net flow in these directions.

3. Particle-phase modelling

3.1. Particle forces

Newton's 2nd law for a particle in a gas is

$$m_p \frac{d v_{p,i}}{dt} = \beta \frac{V_p}{\alpha_p}(v_{f@p,i} - v_{p,i}) + m_p g_i + F_{pw,i} + F_{pp,i} \qquad (3)$$

where m_p is the mass of the particle, $v_{f@p,i}$ is the undisturbed fluid velocity along the particle, $v_{p,i}$ is the particle translational velocity

and β is the drag function as proposed by Wen and Yu (1966), where the reciprocal of the Eulerian fluid-particle timescale is given by

$$\beta = \frac{3}{4} C_D \frac{\alpha_p \alpha_f \rho_f |v_{f@p,i} - v_{p,i}|}{d_p} \alpha_f^{-2.65} \qquad (4)$$

and C_D represents the coefficient of drag for an individual particle and α_f represents the fluid volume fraction. The detailed equation of motion of a particle is provided in Electronic Annex B in the on-line verison of this article. The coefficient of drag, C_D, is defined as (Rowe, 1961)

$$C_D = \begin{cases} \frac{24\left[1+0.15((1-\alpha_p)Re_p)^{0.687}\right]}{Re_p(1-\alpha_p)}, & \text{if } (1-\alpha_p)Re_p < 1000 \\ 0.44, & \text{if } (1-\alpha_p)Re_p \geqslant 1000 \end{cases} \qquad (5)$$

3.2. Particle tracking

Modelling the particle motion in the Lagrangian framework involves tracking the properties of individual particles and the fluid properties at the particle's location. MultiFlow (van Wachem et al., 2012), which is an in-house multiphase code, achieves this by creating a particle mesh. This mesh is isotropic and homogeneous in all Cartesian directions and completely overlaps with the corresponding fluid mesh, see Fig. 1. The particle grid spacing is directly proportional to the mean particle diameter (constant C in Fig. 1, where d_p is the particle diameter). The particle mesh is used to determine the interpolation properties from the fluid phase to the particle phase, as well as to enable collision-neighbour finding lists.

The fluid effects on the particles are modelled using Eq. (3). Including only this effect and neglecting the effect of particles on the fluid and particle–particle interactions is referred to in the literature as one-way coupling. Note that the fluid velocity in Eq. (3) strictly represents the undisturbed fluid velocity of a particle's centre along its trajectory. Strictly speaking this velocity does not exist because of the particle's presence at that point. In the point-particle approach, the fluid velocity at the location of the particle is sim-

Fig. 1. 2D visualisation of individual particle and fluid meshes.

ply found by interpolation. Note that the fluid velocity is in the Eulerian framework and the particles are in the Lagrangian framework. Therefore, it is required to transform the Eulerian fluid properties to Lagrangian at the particle's centre by an interpolation technique. In this work, spline interpolation has been used to interpolate the fluid properties from the fluid mesh to the particle mesh. Yeung and Pope (1988) perform a study on the interpolation schemes in homogeneous turbulence and report that spline (or third order Lagrangian polynomial) interpolation has the least effect (or minimum error) on the fluid energy spectrum. Balachandar and Maxey (1989) investigate the effect of interpolation methods on one-particle and two-particle dispersion in homogeneous turbulence. They also report that spline interpolation offers the highest accuracy and least computational time when compared to other methods, which is important for two-particle dispersion (or coagulation).

The particle effects are included in the fluid momentum equation (Eq. (1)) as a source term approximated by the Wen and Yu (1966) drag function (Eq. (4)). The inclusion of this source term is referred to as two-way coupling. For two-way coupling, the Lagrangian particle properties must be transformed to Eulerian because all properties must be continuous. Interpolation from the particle centres to the particle mesh (and consequently to the fluid mesh) is performed on a volume basis. This is because one particle cell might have several particles and/or several fractions of particles and this leads to different weighting of each particle within each particle cell. The contribution of each particle to the particle mesh (and vice versa) is determined by the fraction of the volume of the particle present in each particle cell and, consequently, in each fluid cell. Therefore, the two-way coupling is the total contribution of all particles and fractions of particles in the fluid cell. The model has two distinct timesteps, corresponding to the particle and the fluid. The two-way coupling term is determined at every particle timestep which is always smaller than the fluid timestep. Thus, the total contribution of the two-way coupling term at the fluid timestep is updated by the cumulative contribution at each particle timestep. When collisions are neglected, the particle time-step is set to a small and fixed value, so it is much smaller than the fluid time-step. Loth (2000) discusses the assumptions required for this approach. Eaton (2009) discusses the relevant difficulties of the point-mass approach in the LES framework. The main assumption of the point-particle approach is that the particle diameter must be smaller than the Kolmogorov micro-scale (η_κ) and smaller than the grid size. Bagchi and Balachandar (2003) investigate the effect of turbulence on the drag and lift of a particle via DNS of an isotropic field. They report that when the particle diameter is within the range $1.5\eta_\kappa < d_p < 10\eta_\kappa$, the drag law is accurately predicted. Moreover, Vreman et al. (2009) mentions that the drag force acting on the particles is reasonably predicted when $d_p < 4\eta_\kappa$. Based on the experimental data concerning this study, the Kolmogorov length scale at the centre of the channel and near the wall are $\eta_{\kappa,centre} = 9.35 \times 10^{-5}$ m and $\eta_{\kappa,wall} = 2.911 \times 10^{-5}$ m. Therefore, throughout the channel in this study this ratio does not exceed $d_p/\eta_\kappa < 7$. Furthermore, Yamamoto et al. (2001) show that for large particle Stokes numbers ($St \gg 1$) the dispersion of particles is not affected by the subgrid scales. Hence, in this study it is not expected that the particle statistics to be affected significantly by the unresolved scales. Moreover, because $\Delta y \geqslant \eta_\kappa$ everywhere in the domain, including in the near-wall region, the assumption that the particle is much smaller than the mesh spacing is also satisfied in this study.

The particle source terms have a different impact on the flow since interpolation is also performed between the particles (their centres) and the particle mesh. Cubic spline interpolation is used to interpolate properties from the vertexes of the particle mesh to the particle centres. The particle mesh also enables the efficient
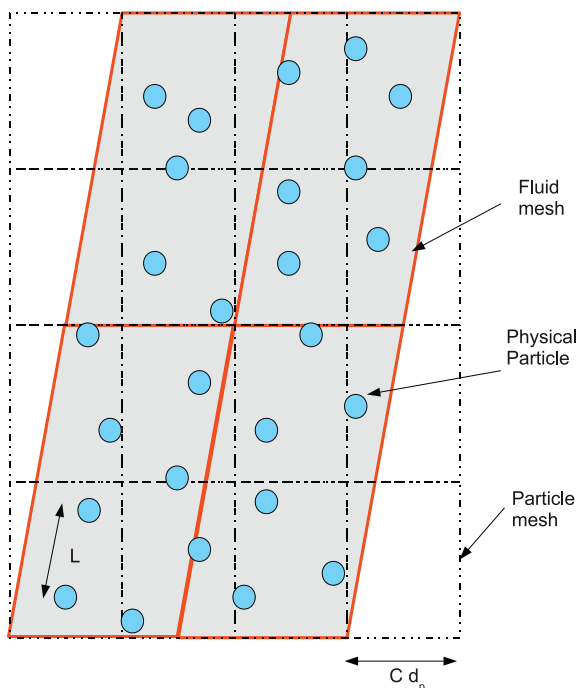
tracking of inter-particle and particle–wall collision pairs (or four-way coupling). The particle mesh significantly reduces the search of possible collision pairs, either between particles or between particles and wall-segments, and hence the computational run-time.

3.3. Inter-particle and particle–wall interactions (four-way coupling)

The interactions of particles with other particles and walls are of dynamic nature. This is because the particle movements are essentially defined by the particle–particle interactions, particle–wall interactions, particle–fluid interactions and/or body forces. Newton's 2nd law is solved for each particle, accounting for these interactions and thus obtaining the individual trajectories (i.e. Lagrangian framework). The integral for the soft sphere model is approximated with the Verlet algorithm (Allen and Tildesley, 1989), whereas for the hard sphere model with an explicit scheme.

The major distinction between the soft sphere and hard sphere models is that the soft sphere collisions are fully resolved. The deformation of the particles undergoing a collision is approximated and the resulting repellent force is determined. This implies that the soft sphere model needs a very small time-step, much smaller than the fluid time-step. In other words, the soft sphere model computes the actual deformation of the particles and the corresponding contact forces which depend on the contact time of the collision. On the other hand, the hard sphere algorithm performs each collision only once since it is approximated as instantaneous. Collisions are treated by evaluating the potential collision time between each pair. Therefore, this framework is so-called event-driven. The hard sphere collisions are resolved by satisfying the global conservation of momentum and only depend on the direction of motion of each particle and their corresponding elapsed collision time. Hence, the operation of the hard sphere algorithm is significantly faster compared to the soft sphere algorithm in fast flowing dilute flows.

3.4. Rough wall modelling

The effect of rough walls has shown to be important in a number of gas-particle flows (Sommerfeld and Kussin, 2004) because the particles that collide with a rough wall have a tendency to be suspended into the flow. In horizontal channel flow simulations, neglecting the effect of wall roughness, a large number of particles *grazing* the wall are predicted. It was shown experimentally by Kussin and Sommerfeld (2002) that the wall roughness strongly enhances the transverse dispersion of the particles and their fluctuating velocities throughout the channel. The measurements have also revealed that the wall roughness causes a significant reduction of the mean horizontal velocity of the particles.

The most obvious approach to model a rough wall is a deterministic approach, where the wall roughness is resolved. However, because of the rapidly changing normal of the wall or the small length scale required to describe the wall roughness, a fully deterministic approach is very costly. Therefore, a stochastic approach to model wall roughness is adopted. There are a number of stochastic approaches described in the literature (for example see Tsuji et al., 1987), the most applied model is of Sommerfeld (1992) and later corrected by Sommerfeld and Huber (1999) for the so-called shadow effect. A stochastic model usually works with a virtual wall concept, which changes the orientation of the wall with a randomly chosen angle roughness γ, see Fig. 2.

The angle γ is sampled according to the following algorithm (Sommerfeld and Huber, 1999):

1. Sample a roughness angle, γ, from a normal distribution. The standard deviation for this distribution is given by the actual roughness of the wall as experienced by the particle.
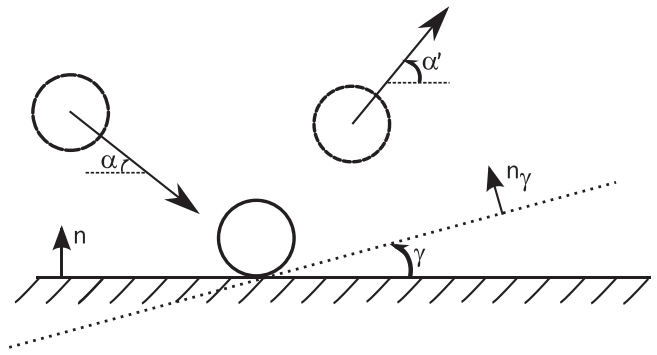

Fig. 2. An illustration of the *virtual wall* approach, in which the macroscopic wall is locally replaced by a virtual wall, which is obtained by rotation under a stochastically sampled angle, γ. The particle pre-collision angle, γ, and post-collision angle, γ' are shown as well.

2. If a negative roughness angle with an absolute value larger than the pre-collision angle, α is sampled, the roughness angle is rejected, as this is a non-physical collision; the so-called *shadow-effect*.
3. Rotate the local solid wall with the random roughness angle, γ and so it has normal $\boldsymbol{n}_\gamma$. This fictitious wall replaces the actual solid wall in determining the collision dynamics.

The above algorithm has been further refined by Konan et al. (2009), by realising that the above algorithm only accounts for a single collision with a rough wall. In the original algorithm of Sommerfeld and Huber (1999), when the post collision angle is very small, a so-called grazing particle is predicted, e.g. a particle which remains close to the wall. However, in reality it is very likely that such a particle will endure a second wall collision very soon after the first collision. This effect decreases the likelihood of random rough wall angles leading to very small post collision angles.

So far, all the employed rough wall models from the literature have dealt with hard sphere type collision models, where the actual collision is assumed instantaneous. The rough wall model can then be used as a black box; using a direct probability density function using the pre-collision angle to predict a post-collision angle. In this work the roughness model of Sommerfeld (1992) with the shadow wall effect is used for the simulations were the particles are considered as hard spheres. However, the algorithm needs to be refined when the particles are considered as soft spheres. This is because the collisions are fully resolved, allowing for a realistic collision time and multiple collisions to occur at the same time.

The important consequence from resolving the collision as it occurs, is the assumption that walls have an infinite size. For instance, a particle colliding with the virtual wall depicted in Fig. 2 might leave the domain at the bottom. In reality, this would not occur because of two reasons. The first reason is that a real rough wall has an amplitude, which is assumed zero in the virtual wall method. The second reason is that a real rough wall segment is of finite length; usually small compared to the particle size. To overcome these two shortcomings in a soft sphere framework, a variation of existing virtual wall procedure is employed:

1. When the shortest particle–wall distance is the wall roughness amplitude (taken to be 10% of the particle diameter) one virtual wall is generated at the point of the particle which is closest to the wall. The virtual wall is generated with the original algorithm (Konan et al., 2009; Sommerfeld and Huber, 1999) as outlined above.
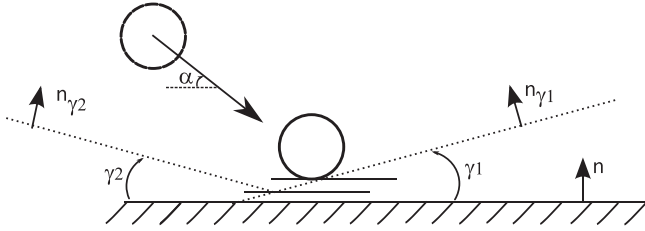
Fig. 3. An illustration of the newly proposed multiple virtual wall approach. A first virtual wall is introduced when the particle reaches the amplitude of the wall roughness added to the actual smooth wall. Additional virtual walls are added randomly every time the particle moves half of this amplitude closer to the wall. One such additional virtual wall is depicted.

2. If the shortest particle–wall distance becomes half of the distance at which the virtual wall was inserted, i.e. the particle has moved closer to the wall, a second virtual wall is introduced, with a newly randomly sampled angle. This is shown in Fig. 3.
3. The addition of new virtual walls is repeated until the particle is moving away from the wall.

The required standard deviation for the normal distribution is taken from the experimental data provided by Kussin and Sommerfeld (2002). In the analysed flow, up to three virtual walls are required to deal with the rough wall collision, although almost all collisions are dealt with by application of the first rough wall.

4. Simulation set-up

4.1. Set-up

The large-scale simulations are performed in the Eulerian–Lagrangian framework and the predictions are compared to the experimental work of Kussin and Sommerfeld (2002). In their work, a horizontal channel with a height of 35 mm, a width of 175 mm and a length of 6 m, corresponding to approximately 170 channel heights, is used. A flow of an air-particle mixture with various particle sizes and mass loadings is introduced in the horizontal direction.

This paper focuses on the results obtained for the single phase flow and the two-phase flow with mass loading ϕ = 1.0, which is based on the experimental conditions. At this mass loading both fluid-particle as well as particle–particle interactions are expected to be important. The experimental Reynolds number considered based on the channel height is 42,585, arising from the average air velocity of U_{av} = 19.7 m/s, air density of ρ_f = 1.15 kg/m^3 and a viscosity of μ_f = 18.62 Pa s. The friction Reynolds number based on the half channel height is Re_τ = 600. The particles considered are glass beads, ρ_p = 2500 kg/m^3, with an average diameter of 195 μm and a narrow particle size distribution as described in Kus-

sin and Sommerfeld (2002). In the simulations, particles are tracked for 47 T_L, where T_L is the integral time scale of turbulence at the centre of the channel. In the Electronic Annex C in the online version of this article the various particle properties and Stokes numbers based different fluid timescales are presented. It is important to note that the Stokes number of the particles for all definitions is greater than one.

The domain used for the simulations is sketched in Fig. 4. The simulations are carried out with our in-house code MultiFlow (van Wachem et al., 2012; Bruchmüller et al., 2011), which is a fully coupled parallel computational fluid dynamics code based on finite volume discretisation. The simulations are carried out in a three-dimensional domain of 0.175 m × 0.035 m × 0.035 m, where the X direction corresponds to the direction of the flow and the negative Y direction is the direction of gravity. The X and Z directions are taken to be periodic.

4.2. Initial and boundary conditions

The flow is initialised by setting a mean velocity corresponding to the mass flow rate of the experimental data provided by Kussin and Sommerfeld (2002). On top of the mean, synthesised turbulence is added as randomly sampled from a von Karman spectrum, using the Fourier modes of a fully developed turbulent spectrum. The initial condition does not impose a flow profile; the flow profile is formed as a result of solving the Navier–Stokes equations and enforcing the no-slip condition for velocity at the wall. The boundary conditions at the wall are set as no-slip.

For the simulations involving particles, the particles are introduced uniformly in the domain with a small random slip velocity compared to the local fluid velocity. The number of particles in the domain, which is determined from the mass loading of ϕ = 1.0, given in the experimental set-up, is 24,500, leading to a particle volume fraction of α_p = 4.7977 × 10^{-4}. The experimental data provided by Kussin and Sommerfeld (2002) have a slightly different mass flow rates for the single phase and particle laden cases. The forcing term (see Eq. (2)) keeps a constant mass flow rate of $\dot{m}$ = 0.028175 kg/s for the single phase and $\dot{m}$ = 0.027044 kg/s for the particle laden cases, computed from the data provided by Kussin and Sommerfeld (2002). The resulting pressure drop equals the integrated wall shear stress in the channel. In addition, the pressure is fixed to a reference value on one arbitrary cell face inside the domain. In the Electronic Annex A, spectra for the one dimensional spanwise and streamwise velocities are included in order to ensure that the LES simulations in this study resolve most of the energetic lengthscales.

4.3. Computational mesh

Two computational meshes are used to carry out the single-phase simulations in order to show that the solution is grid independent. The coarse geometry is then used to carry out the gas-
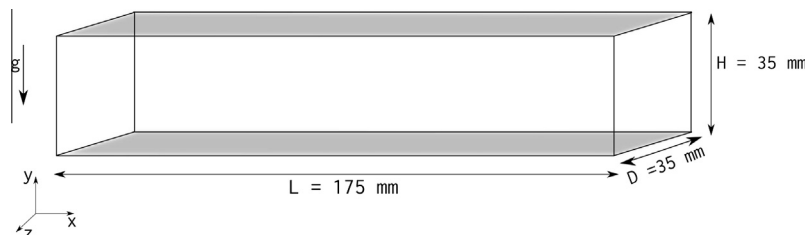

Fig. 4. The geometry of the channel as used in the simulations. The mean flow is in the X direction and the gravity is in the Y direction. Both the X and Z directions are periodic for the flow and the particles. The solid walls of the channel are indicated in grey.

particle simulations. The coarse mesh contains a total of 870,000 computational cells and the finer mesh contains a total of 1,299,000 computational cells. The refinement is achieved by refining the nodal spacing equally in all directions. Both meshes resolve the wall boundary layer, and contain 5 and 12 mesh points within the $y^+ = 10$ layer, respectively. Near the wall a DNS resolution is obtained by using

$$y = y_{max} \left[\frac{1}{2} \left[\frac{1 + \tanh \left(R \frac{y}{y_{max}} - \frac{1}{2} \right)}{\tanh \left(\frac{1}{2} R \right)} \right] \right] \tag{6}$$

where R is a constant set to 7.0 and defines the amount of refinement near the wall. $y_{max} = 35.0$ mm, is the channel height. In addition, in every $x^+ = 50$ and $z^+ = 30$, 1 mesh point is uniformly added.

4.4. Discretisation

The discretisation of the Navier–Stokes equations is done using a finite volume approach, combined with a second order accurate three point backward Euler time discretisation for the temporal terms and a second order accurate central differencing scheme for the advection term. The pressure velocity coupling is done in a fully coupled framework, using one outer iteration per time-step (van Wachem et al., 2007).

5. Results and discussion

Single-phase simulations are performed in order to validate the performance of the LES models. The Smagorinsly model with van Driest dampening and the dynamic model are compared with the experimental data. The single-phase results are in very good agreement with the corresponding experimental data. Additionally, in order to verify that the numerical solution is grid independent, mesh refinement is performed. The results show that the solution is indeed grid independent. The interested reader is refered to the Electronic Annex A in the online version of this article.

5.1. Particle laden simulations

Particle laden simulations are carried out and compared to the experimental work of Kussin and Sommerfeld (2002). The effects of wall roughness, one-way, two-way and four-way coupling are investigated and compared.
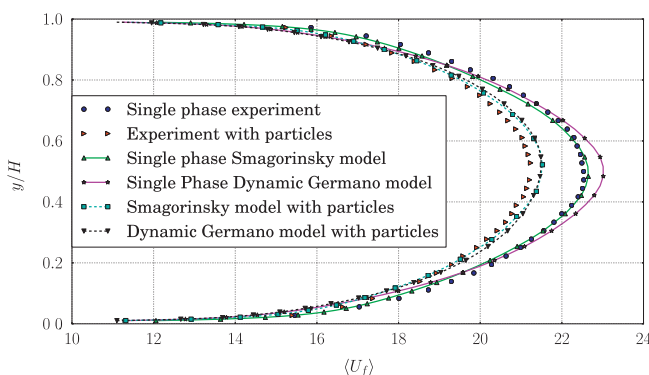
5.2. Choice of LES model for fully coupled particle laden simulations

The purpose of this section is to investigate the effect of the subgrid scale models when used in conjunction with the fully coupled simulations. Fully coupled simulations with the Smagorinsky model with van Driest dampening and the Dynamic Germano model are performed and compared to the particle-laden experimental data. Yamamoto et al. (2001), who perform LES simulations of a vertical particle-laden channel flow, question the suitability of the Dynamic Germano model. The Dynamic Germano model, which utilises plane averaging in order to be numerically stable, can be affected erroneously by the anisotropy caused by the particles. This violates the assumptions of the model.

Fig. 5 compares the mean horizontal velocity predicted by the two subgrid scale models. Fig. 5 shows that the Smagorinsky model with van Driest dampening is closer to the experimental particle-laden mean horizontal velocity. Additionally, the Dynamic Germano model modulates turbulence by a higher percentage compared to the Smagorinsky model with van Driest dampening, see Fig. 6. Note that Kuerten (2006) investigates the effects of subgrid scale models on the particle statistics and reports that the mean particle wall-normal (i.e. horizontal) velocity is least accurate compared to the DNS results. Based on these results, the Smagorinsky model is chosen for the remaining sections of this paper.

5.2.1. Effect of wall roughness

Fig. 7 compares the horizontal mean fluid velocity with the experimental data both for smooth and rough walls. Similarly to the single phase simulations the results for the rough walls are
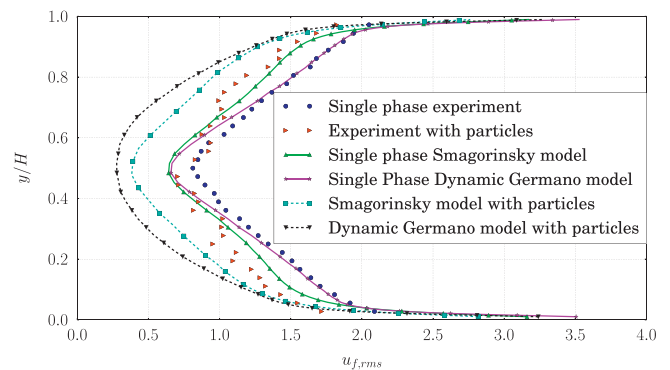
Fig. 6. The horizontal fluid velocity fluctuations for the single phase fluid and particle-laden fluid as a function of dimensionless channel height for the Dynamic Germano and Smagorinsky LES models compared to the experiments.
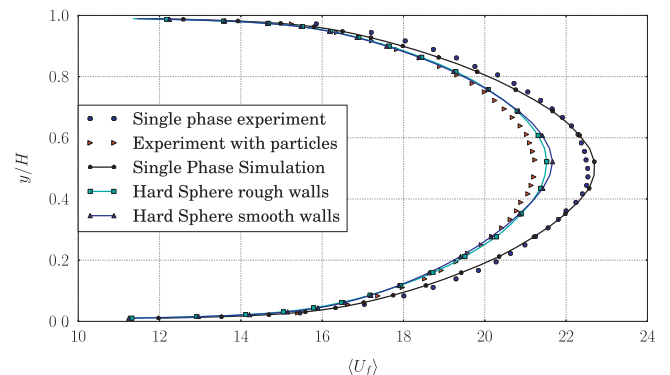
Fig. 5. The horizontal mean fluid velocity for the single phase fluid and particle-laden fluid as a function of dimensionless channel height for the Dynamic Germano and Smagorinsky LES models compared to the experiments.

Fig. 7. The horizontal mean fluid velocity for the particle-laden fluid as a function of dimensionless channel height for the hard sphere model with rough walls and smooth walls compared to the experiments.
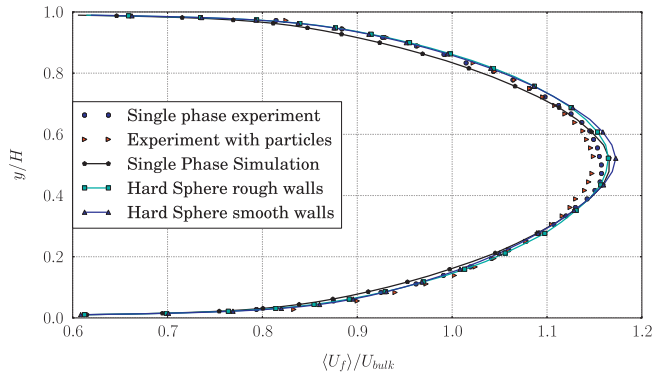
Fig. 8. The dimensionless horizontal mean fluid velocity for the particle-laden fluid as a function of dimensionless channel height for the hard sphere model with rough walls and smooth walls compared to the experiments.

Fig. 10. The shear stress for the particle-laden fluid as a function of dimensionless channel height for the hard sphere model with rough walls and smooth walls compared to the experiments.

slightly over-predicted at the centre of the channel compared to the experimental data. One possibility for this small discrepancy is that the experimental data have a small mean velocity in the vertical direction, which implies that the flow in the experiment is not fully developed. The mean vertical velocity is small, on the order of 1.6% compared to the mean horizontal velocity. Another possibility is that the effect of the sub-grid scales is ignored and this may have a small effect on the flow as well. It is interesting to note that when the walls are treated as rough the mean fluid velocity is similar to the particle-free experimental results. Fig. 8 shows the dimensionless mean horizontal velocities as a function of dimensionless height. This means that the average mean fluid velocity shape is not influenced by the presence of the particles, although the simulations predict a small effect of the particles on the flow.

Additionally, the simulated flow profile for the particle laden cases without wall roughness shows a slight asymmetry. This is because more particles are found in the bottom half of the channel, lowering the fluid velocity in this region due to the effect of two-way coupling. Although there is no experimental data for this precise case, a similar observation was made by Lain et al. (2002), who experimentally and numerically investigate the four-way coupling of a particle-laden horizontal channel flow for similar experimental conditions.

The experimental particle-free and particle-laden RMS velocities have small differences between them, as shown in Fig. 9, which compares the fluid horizontal velocity fluctuations. On the other hand, the simulation results show larger differences in RMS velocities. The simulations predict a large attenuation of the turbulence in the channel flow due to the addition of particles. Therefore, the predicted particle-laden velocity fluctuations are lower compared
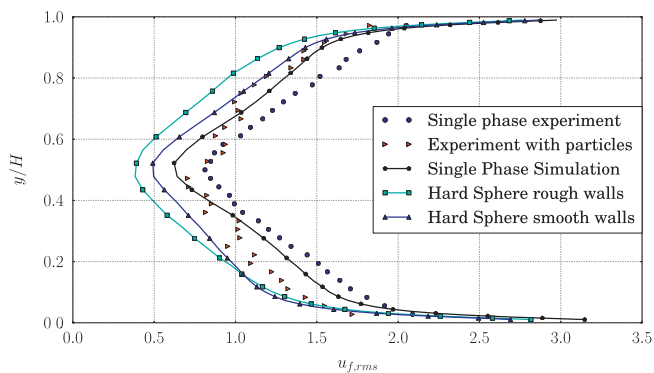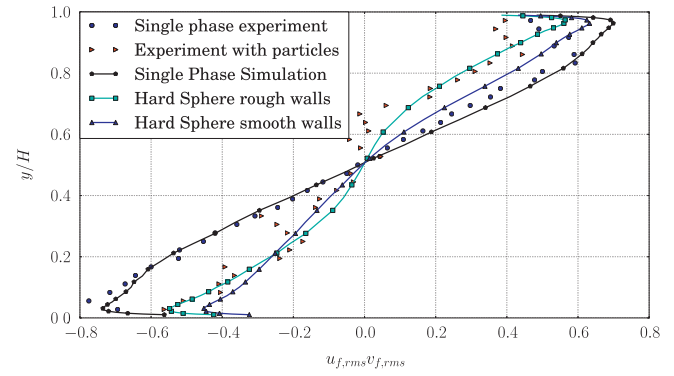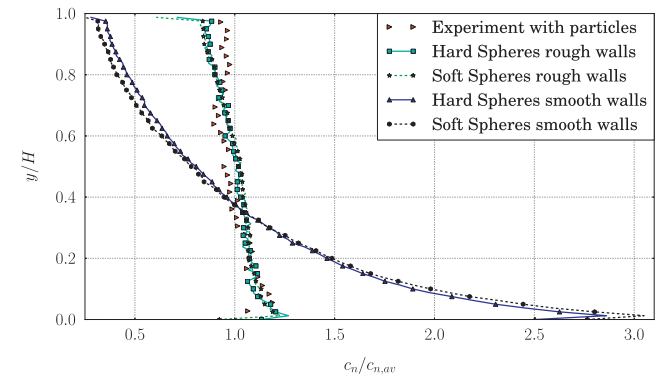

Fig. 11. The particle concentration as a function of dimensionless channel height for the hard sphere and soft sphere models with rough walls and smooth walls compared to the experiments.

to the corresponding experimental results. This shows that the two-way coupling over-dampens turbulence by 25% at the centre of the channel.

This is opposite to the findings of Eaton (2009), who reports that the two-way coupled simulations do not attenuate turbulence sufficiently. In fact, Eaton (2009) mentions that by ten-folding the mass loading (i.e. by adding more particles) the correct turbulence attenuation is achieved. Eaton (2009) has not provided a physical explanation for this. Yamamoto et al. (2001), who perform LES simulations on a vertical channel, mention that for large Stokes numbers their computations for turbulence attenuation do not agree with the experimental results. For small Stokes numbers, however, Yamamoto et al. (2001) mention that the predicted turbulence attenuation is in good agreement with the experimental results.

The shape of the predicted horizontal RMS velocity of the particle-laden case compared to the single phase case is also somewhat different. The shape of the single-phase horizontal RMS velocity, as predicted by the simulations, are symmetric. On the other hand, the corresponding particle-laden case shows a slight asymmetry in the RMS fluid velocity. This is because without the wall roughness more particles tend to remain near the bottom of the channel, and most graze in a layer near the bottom. This influences the fluid RMS velocity profile due to the two-way coupling, which makes it asymmetric as opposed to the symmetric profile as predicted for the rough wall case. In the smooth wall case, the rebound angle of the particles is smaller compared to the rough wall case. Thus less particles are found at the centre of the channel which would then be dispersed by the turbulence to other parts of the channel,

Fig. 9. The horizontal rms fluid velocity for the particle-laden fluid as a function of dimensionless channel height for the hard sphere model with rough walls and smooth walls compared to the experiments.

e.g. the top wall. The smooth walls fail to do this and due to the action of gravity, the particles tend to remain near the bottom wall. Turbulence is more suppressed at the bottom half of the channel due to the high particle volume fraction and two-way coupling, thus creating an asymmetric RMS velocity profile. As also mentioned by Lain et al. (2002), this effect is more pronounced with increasing mass loading. Additionally, this behaviour has important consequences on the shear stresses, which are plotted in Fig. 10. The shear stresses on the wall for the smooth wall case are asymmetric, opposed to the rough wall case and the single phase case, e.g. at $y/H = 0.05$, $u_{f,rms}v_{f,rms} = -0.45$ but at $y/H = 0.95$, $u_{f,rms}v_{f,rms} = 0.65$.

This is also illustrated in Fig. 11, which compares the particle concentration obtained by the simulation with the rough and smooth walls with the experimental data. For both the soft and hard sphere models simulating smooth walls, the concentration of the particles is much higher at the bottom wall. However, when the walls are treated as rough, the particle concentration is almost homogeneous and is in very good agreement with the experimental data. The wall roughness, therefore, is important as it helps to redistribute the particles into the main flow.

The redistribution of particles is also driven by particle–particle collisions, even in this dilute case; where the particle volume fraction is $\alpha_p = 4.7977 \times 10^{-4}$. To illustrate this, Fig. 12 compares the particle concentration for rough walls with and without inter-particle collisions. When inter-particle collisions are not taken into account, the particle concentration at the bottom wall is 16.6% higher, despite accounting for wall roughness. In addition, the particle concentration gradient without particle–particle collisions at the centre of the channel is steeper by about 37%. This illustrates the importance of particle–particle collisions even at very low particle volume fractions.

Fig. 13 shows the instantaneous distribution of particles for simulations with: (a) with particle–particle collisions and wall roughness, (b) with no particle–particle collisions and wall roughness (c) with particle–particle collisions and smooth walls, and (d) with no particle–particle collisions and smooth walls. Fig. 13a–c illustrate that the particles remain suspended in the channel, however with a different concentration profile. On the other hand, when particle–particle collisions are ignored and the walls are treated as smooth, particles with time slowly migrate to the bottom wall and remain there. In fact the flow now resembles sediment transport because the particles are now sliding across the bottom wall. The importance of the inter-particle collisions in redistributing the particles in the channel becomes apparent. Vreman et al. (2009) numerically investigate the effect of particle–particle collisions for a vertical channel, but at a much lower Re
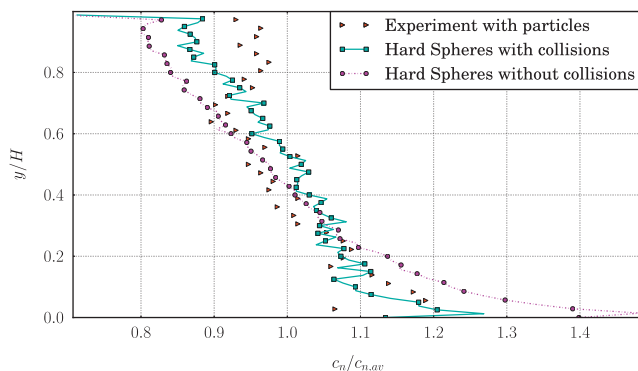
Fig. 13. Instantaneous distribution of particles for simulations when the statistics have reached steady state, (a) with particle–particle collisions and wall roughness, (b) with no particle–particle collisions and wall roughness (c) with particle–particle collisions and smooth walls, and (d) with no particle–particle collisions and smooth walls.

number and much higher mass loading. They report that the collisions affect the statistics of both the fluid and the particles. They conclude that it is important to include the particle–particle collisions in order to correctly predict the modification of the fluid and particle statistics. Yamamoto et al. (2001) investigate the particle–particle collisions at lower mass loadings and reach similar conclusions.

On the other hand, particles remain distributed across the channel when inter-particles collisions are taken into account even for the smooth walls (see Fig. 11), whereas this is not true when inter-particle collisions are ignored. Therefore, inter-particle collisions act as an extra distributive mechanism, even for dilute flows. This is an important finding because many simulations in the literature ignore inter-particle collisions because of the low mass loading. Lain and Sommerfeld (2010) investigate the transport of particles in a cylindrical elbow of mass loading ratio 0.7 and illustrate that by ignoring the particle–particle collisions, particles do not preferentially concentrate at the exit of the elbow. Therefore the roping effect is not observed, however, when Lain and Sommerfeld (2010) perform fully coupled simulations indeed observe this effect. This indicates that particle–particle collisions are especially important in all wall-bounded flows.

Fig. 12. The particle concentration as a function of dimensionless channel height for the hard sphere model with and without inter-particle collisions (with rough walls) compared to the experiments.
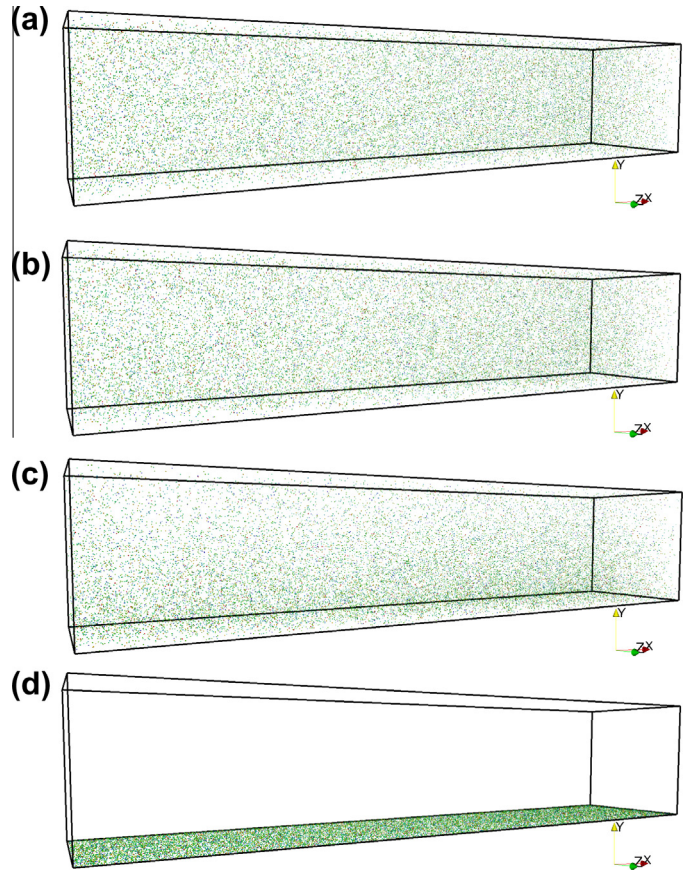
5.2.2. Effect of hard sphere and soft sphere models on the particle statistics

As already discussed, in dilute flows the choice between the hard sphere and soft sphere models largely depends on the compu-
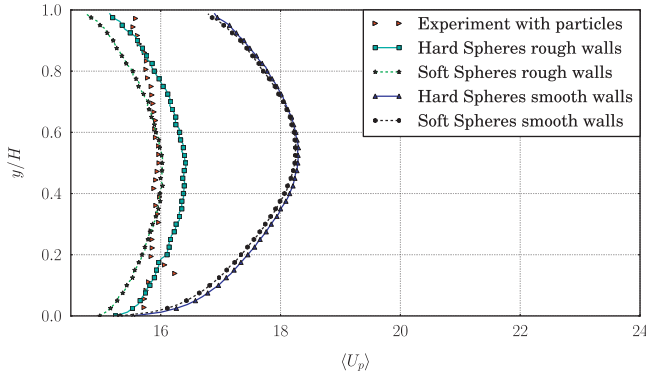
Fig. 14. The horizontal mean particle velocity as a function of dimensionless channel height for the hard sphere and soft sphere models with rough walls and smooth walls compared to the experiments.
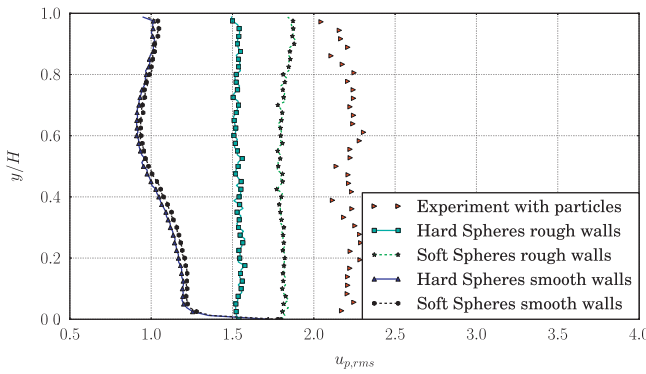

Fig. 16. The horizontal mean particle velocity as a function of dimensionless channel height for the hard sphere model with rough walls and smooth walls with different tangential coefficients of restitution compared to the experiments.

Fig. 15. The horizontal RMS particle velocity as a function of dimensionless channel height for the hard sphere and soft sphere models with rough walls and smooth walls compared to the experiments.
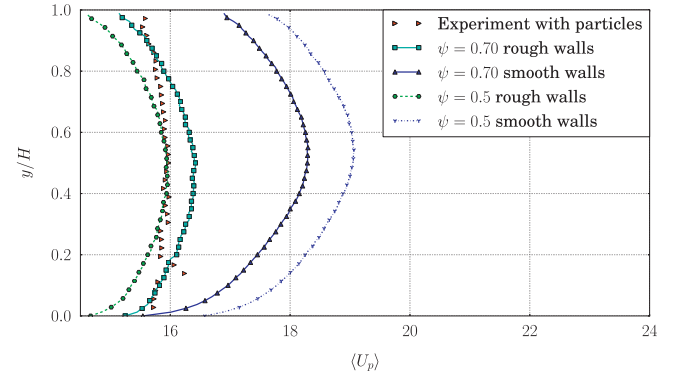

Fig. 17. The horizontal RMS particle velocity as a function of dimensionless channel height for the hard sphere model with rough walls and smooth walls with different tangential coefficients of restitution compared to the experiments.
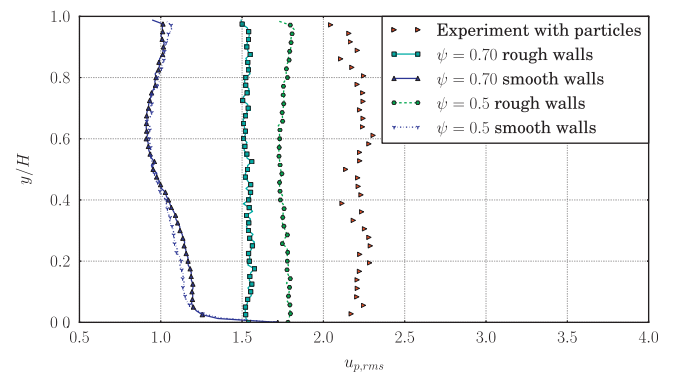
tational time spent to solve the particle equation of motion. For very dilute flows, the hard sphere model is the most natural choice. However, when the collisions can no longer be assumed as binary and instantaneous, the soft sphere model is the only realistic option. It is interesting to know whether the choice of the collision model affects the statistics. Fig. 14 compares the mean velocity obtained from both models with the experimental data. The same comparison is performed for the smooth walls. The differences between the hard and soft sphere models for the smooth walls are almost negligible. However, the differences between the hard and soft sphere models for the rough walls are minor. This is because the rough wall treatment in the soft sphere implementation adds extra virtual walls during the collision of a particle with a wall, which is a more realistic representation of a rough wall compared to the hard sphere rough wall treatment where one random wall is considered. This is because, a soft sphere collision is not instantaneous and occurs over a finite amount of time. Similarly, the same effects are observed on the fluid statistics. However, Fig. 15, which compares the particle velocity fluctuations, shows that the differences are somewhat larger. Additionally, the differences in both particle mean and RMS velocity profiles are because the hard sphere collisions are unfortunately heavily dependent on the tangential coefficient of restitution (ψ); the effects by varying this quantity are shown in Figs. 16 and 17.

This tangential coefficient of restitution is empirical and difficult to evaluate experimentally. Therefore, a sensitivity analysis is essential to determine an appropriate value of ψ in order to obtain good agreement with the experimental data. Konan et al. (2011), who perform an investigation based on DES; use particles

with a diameter of $100\mu m$ with similar flow settings, report that similar results can be obtained by increasing the experimental roughness angle (γ) from 5.3 to 6.5. This is another way of changing the effect of ψ because it affects the particle rebound angle directly. Konan et al. (2011), however, neglect the effect of the rotation of particles and use the collision model proposed by Sommerfeld and Huber (1999). This model does not split the coefficient of restitution into normal and tangential coefficients but has a single coefficient of restitution which depends only on the impact angle of the particles and it is this relationship that is determined empirically. Moreover, the coefficient of friction is treated the same way, i.e. it is a function of impact angle. In this work the roughness angle used is $\gamma = 5.02^o$ estimated from the experimental measurements and reported by Sommerfeld and Huber (1999) and Lain et al. (2002). The soft sphere parameters rely on the properties of the solids and no empiricism is required. Most importantly, the coefficient of restitution is related to the parameter α (see Tsuji et al., 1992) and automatically depends on impact velocity and angle. Tsuji et al. (1992) heuristically find a relation for the coefficient of restitution which is independent of the constants used in the soft sphere model, which is not required to be empirically specified.

5.2.3. Effect of one-way coupling

To investigate the effect of one-way coupling on the fluid and particle statistics the particle sources in the fluid momentum equation are "turned off"; i.e. by making the last term on Eq. (1) equal to zero and setting the fluid volume fraction as $\alpha_f = 1.0$. One-way coupled simulations are performed under the same conditions for both
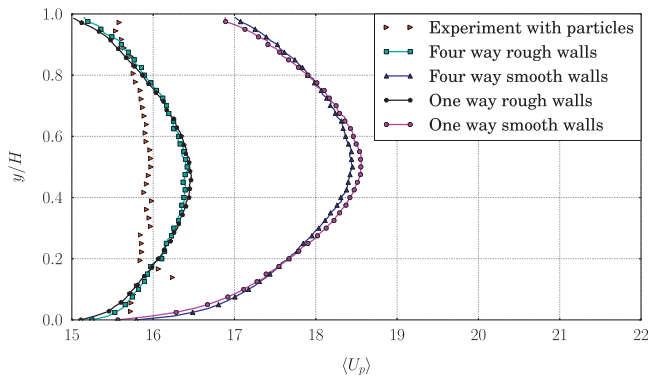
Fig. 18. The horizontal mean particle velocity as a function of dimensionless channel height for the four-way and one-way coupled simulations with rough walls and smooth walls to the experiments.

Fig. 19. The horizontal RMS particle velocity as a function of dimensionless channel height for the four-way and one-way coupled simulations with rough walls and smooth walls to the experiments.
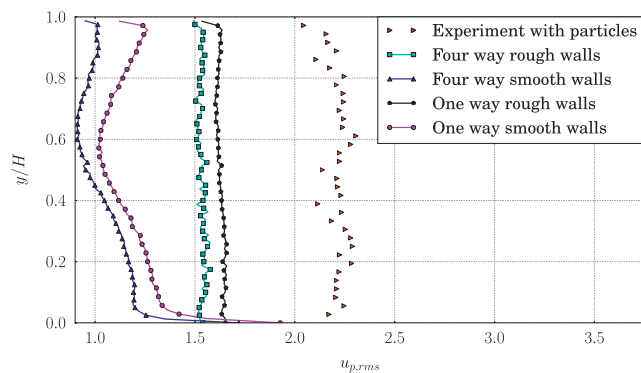
rough and smooth walls. The particle mean velocity profile, presented in Fig. 18, is not affected. The differences are statistically insignificant because the difference, for example, of the mean centre-line particle velocity is less than 0.8%. This is because the particle volume fraction is very low, so the two-way coupling force does not affect the average particle velocity. Therefore, the absence of the two-way coupling does not significantly affect the average particle statistics. The particle concentration profiles, not presented, are almost identical compared to the four-way coupled simulation. On the other hand, the particle velocity fluctuations exhibit different trends. Fig. 19 compares the particle RMS velocity fluctuations in one-way coupled simulations and fully coupled simulations, for both types of walls. The one-way coupled RMS velocity values are higher compared to the respective fully-coupled simulations. In particular, the fluctuations predicted by the one-way coupled simulations and by considering the walls as rough are 10% higher.

6. Conclusions

This work compares different models and their implications in the framework of LES and compares the findings to the experimental results for turbulent particle-laden channel flow of Kussin and Sommerfeld (2002). The Reynolds number of the simulations is approximately 42,000 based on the full channel height and the mass loading of the simulations is 1.0, as set by the experiment, corresponding to about 24,500 particles. Mesh refinement studies show that the fully converged solutions are in very good agreement with the single-phase experiments. Also, the results obtained from employing the standard Smagorinsky LES model are very sim-

ilar to the dynamic Germano-Lilly model. For the multiphase cases, the results of fully-coupled simulations are compared to one-way coupled and two-way coupled simulations and their differences are physically interpreted. In addition, the soft sphere and hard sphere particle collision algorithms are compared. The effect of the wall roughness on the particle statistics is also investigated and a new roughness model is proposed in order to be used with the soft sphere methodology.

The predicted particle-laden results for average fluid and particle velocity are in very good agreement with the experimental findings. The predicted particle-laden fluid fluctuations are slightly lower compared to the particle-laden fluid fluctuations of the experimental data. Although the gas–solid flow is relatively dilute, there is a major difference between the results obtained by the one-way coupled and the two-way coupled models, having a particularly large effect on the particle velocity fluctuations. The particle velocity fluctuations show an almost 10% difference between the one-way and two-way coupled approach.

The results obtained with the soft sphere (discrete element model) and hard sphere (event-driven) models are also compared. The simulation results show that the two models yield almost identical fluid velocity statistics. The particle mean and RMS velocity profiles are somewhat different, which is attributed to the dependence of the hard sphere model on empirical properties. In particular, a parameter sensitivity analysis on the tangential coefficient of restitution for the hard sphere model is performed in order to obtain good agreement with the available experimental data. On the other hand, the soft sphere model, which is independent of empirical parameters, does not require a sensitivity analysis. Additionally, the particle statistics may be different due to the treatment of the rough walls in the two models. In the soft sphere methodology, a new model is proposed to account for the wall roughness, as the collision of a particle occurs over a finite amount of time. The results show that the newly proposed model for treating the rough walls in the soft sphere methodology are in very good agreement with the experimental data.

The wall roughness in the case researched has a very big effect on the gas-particle flow. In cases where wall roughness is accounted for, the average rebound angle of the particles colliding with the bottom wall is slightly larger than in the case considering fully smooth walls. This slightly larger angle enables the particles to re-entrain the bulk of the flow, instead of remaining near the bottom; a so-called grazing particle. Simulations without considering the rough walls show a much steeper particle concentration profile compared to particles in the channel including the effect of rough walls. Due to two-way coupling, the fluid velocity fluctuations and shear stresses are strongly affected because of the large number of particles in the lower part of the channel. In particular, the fluid RMS velocity profiles are asymmetric for the simulations without considering wall roughness, as opposed to the simulations with rough walls. The latter show almost symmetrical flow profiles. Moreover, the large concentration of particles in the bottom half of the channel suppresses the turbulence.

This paper also shows the importance of particle–particle collisions in the relatively dilute gas-particle laden flow. Including the effect of particle–particle collisions increases the re-distribution of particles into the flow, having a similar, although slightly less pronounced, effect as the rough walls. The simulations results in this paper show the importance of four-way coupling and including a model to account for the wall roughness. The overall comparison with the experimental results is very good.

Appendix A. Supplementary material

Supplementary data associated with this article can be found, in the online version, at http://dx.doi.org/10.1016/j.ijmultiphaseflow.2013.02.007.

References

Allen, M.P., Tildesley, D.J., 1989. The Computer Simulation of Liquids, vol. 42. Oxford University Press.

Bagchi, P., Balachandar, S., 2003. Effect of turbulence on the drag and lift of a particle. Phys. Fluids 15, 3496.

Balachandar, S., Maxey, M.R., 1989. Methods for evaluating fluid velocities in spectral simulations of turbulence. J. Comput. Phys. 83, 96–125.

Bruchmüller, J., van Wachem, B., Gu, S., Luo, K., 2011. Modelling discrete fragmentation of brittle particles. Powder Technol. 208, 731–739.

Cundall, P., Strack, O.D.L., 1979. A discrete numerical model for granular assemblies. Géotechnique 29, 47–65.

Eaton, J.K., 2009. Two-way coupled turbulence simulations of gas–particle flows using point–particle tracking. Int. J. Multiphase Flow 35, 792–800.

Elghobashi, S., Truesdell, G.C., 1992. Direct simulation of particle dispersion in a decaying isotropic turbulence. J. Fluid Mech 242, 655–700.

Germano, M., Piomelli, U., Moin, P., Cabot, W.H., 1991. A dynamic subgrid-scale eddy viscosity model. Phys. Fluids A 3, 1760–1765.

Konan, N., Kannengieser, O., Simonin, O., 2009. Stochastic modeling of the multiple rebound effects for particlerough wall collisions. Int. J. Multiphase Flow 35, 933–945.

Konan, N., Simonin, O., Squires, K.D., 2011. Detached eddy simulations and particle Lagrangian tracking of horizontal rough wall turbulent channel flow. J. Turbul. 12, 1–21.

Kuerten, J.G.M., 2006. Subgrid modeling in particle-laden channel flow. Phys. Fluids 18, 025108.

Kussin, J., Sommerfeld, M., 2002. Experimental studies on particle behaviour and turbulence modification in horizontal channel flow with different wall roughness. Exp. Fluids 33, 143–159.

Lain, S., Sommerfeld, M., 2010. Euler/Lagrange computations of particle-laden gas flow in pneumatic conveying systems. In: 7th International Conference on Multiphase Flow, Tampa, FL USA.

Lain, S., Sommerfeld, M., Kussin, J., 2002. Experimental studies and modelling of four-way coupling in particle-laden horizontal channel flow. Int. J. Heat and Fluid Flow 23, 647–656.

Lilly, D., 1992. A proposed modification of the Germano subgridscale closure method. Phys. Fluids A 4, 633–635.

Loth, E., 2000. Numerical approaches for motion of dispersed particles, droplets and bubbles. Prog. Energy Combust. Sci. 26, 161–223.

Louge, M.Y., 1994. Computer simulations of rapid granular with a flat, frictional boundary flows of spheres interacting. Phys. Fluids 6, 2253–2269.

Maw, N., Barber, J.R., Fawcett, J.N., 1976. The oblique impact of elastic spheres. Wear 38, 101–114.

Rowe, P.N., 1961. Drag forces in a hydraulic model of a fluidized bed, part II. Trans. Inst. Chem. Eng. 39, 175–180.

Smagorinsky, J., 1963. General circulation experiments with the primitive equations. I: The basic experiment. Month. Weath. Rev. 91, 99–165.

Sommerfeld, M., 1992. Modelling of particle–wall collisions in confined gas–particle flows. Int. J. Multiphase Flow 18, 905–926.

Sommerfeld, M., 2001. Validation of a stochastic Lagrangian modelling approach for inter-particle collisions in homogeneous isotropic turbulence. Int. J. Multiphase Flow 27, 1829–1858.

Sommerfeld, M., Huber, N., 1999. Experimental analysis and modelling of particle–wall collisions. Int. J. Multiphase Flow 25, 1457–1489.

Sommerfeld, M., 2003. Analysis of collision effects for turbulent gas–particle flow in a horizontal channel. Part II: Integral properties and validation. Int. J. Multiphase Flow 29, 701–718.

Sommerfeld, M., Kussin, J., 2004. Wall roughness effects on pneumatic conveying of spherical particles in a narrow horizontal channel. Powder Technol. 142, 180–192.

Tsuji, Y., Morikawa, Y., Tanaka, T., 1987. Numerical simulation of gas–solid two-phase flow in a two-dimensional horizontal channel. Int. J. Multiphase Flow 13, 671–684.

Tsuji, Y., Tanaka, T., Ishida, T., 1992. Lagrangian numerical simulation of plug flow of cohesionless particles in a horizontal pipe. Powder Technol. 71, 239–250.

Vreman, B., Geurts, B., Deen, N., Kuipers, J., Kuerten, J., 2009. Two- and four-way coupled EulerLagrangian large-eddy simulation of turbulent particle-laden channel flow. Flow, Turbul. Combust. 82, 47–71.

van Wachem, B., Benavides, A., Gopala, V., 2007. A coupled solver approach for multiphase flow problems. In: 6th International Conference on Multiphase Flows 2007, Leipzig, Germany.

van Wachem, B., Zastawny, M., Mallouppas, G., Zhao, F., Denner, F., Pennefather, J.C., 2012. <http://www.multiflow.org/>.

Wen, C.Y., Yu, Y.H., 1966. A generalized method for predicting the minimum fluidization velocity. AIChE J. 12, 610–612.

Yamamoto, Y., Potthoff, M., Tanaka, T., Kajishima, T., Tsuji, Y., 2001. Large-eddy simulation of turbulent gasparticle flow in a vertical channel: effect of considering inter-particle collisions. J. Fluid Mech. 442, 303–334.

Yeung, P., Pope, S., 1988. An algorithm for tracking fluid particles in numerical simulations of homogeneous turbulence. J. Comput. Phys. 79, 373–416.